Title:

A member of the OSCA/TMEM63 family of mechanosensitive calcium channels participates in cell wall integrity maintenance in *Aspergillus nidulans*.

Authors names and affiliations:

Terry W. Hill [a,b,*], Stanley Vance, Jr. [c,†], Jennifer F. Loome [b,†], Benard J. Haugen [b,†], Darlene M. Loprete [b,c], Shana V. Stoddard [b,c], and Loretta Jackson-Hayes [b,c]

[a] Department of Biology, Rhodes College, Memphis, TN 38112 USA

[b] Biochemistry and Molecular Biology Program, Rhodes College, Memphis, TN 38112 USA

[c] Department of Chemistry, Rhodes College, Memphis, TN 38112 USA

[*] Corresponding author at: Department of Biology, Rhodes College, 2000 North Parkway, Memphis, TN, 38112 USA. +1 901 843 3559.

Email Address: hill@rhodes.edu (T. W. Hill)

[†] Contributions of undergraduate co-authors are listed in Supplementary Document 1.

Abstract

The *calF*7 mutation in *Aspergillus nidulans* causes hypersensitivity to the cell wall compromising agents Calcofluor White (CFW) and Congo Red. In this research we demonstrate that the *calF*7 mutation resides in gene AN2880, encoding a predicted member of the OSCA/TMEM63 family of transmembrane glycoproteins. Those members of the family whose physiological functions have been investigated have been shown to act as mechanosensitive calcium transport channels. Deletion of AN2880 replicates the CFW hypersensitivity phenotype. Separately, we show that CFW hypersensitivity of *calF* deletion strains can be overcome by inclusion of elevated levels of extracellular calcium ions in the growth medium, and, correspondingly, wild type strains grown in media deficient in calcium ions are no longer resistant to CFW. These observations support a model in which accommodation to at least some forms of cell wall stress is mediated by a calcium ion signaling system in which the AN2880 gene product plays a role. The genetic lesion in *calF*7 is predicted to result in a glycine-to-arginine substitution at position 638 of the 945-residue CalF protein in a region of the RSN1_7TM domain that is highly conserved amongst filamentous fungi. Homology modeling predicts that the consequence of a G638R substitution is to structurally occlude the principal conductance pore in the protein. GFP-tagged wild type CalF localizes principally to the Spitzenkörper and the plasma membrane at growing tips and forming septa. However, both septation and hyphal morphology appear to be normal in *calF*7 and AN2880 deletion strains, indicating that any role played by CalF in normal hyphal growth and cytokinesis is dispensable.

Keywords:

Cell wall integrity, calcium, OSCA/TMEM63 proteins, DUF221 proteins, protein modeling

1. Introduction

In earlier work (Hill et al., 2006), we identified the *calF*7 mutation in the filamentous fungus *Aspergillus nidulans*, which confers hypersensitivity to agents that compromise cell wall integrity, and here we report that the *calF*7 mutation resides in a locus predicted to encode a protein belonging to the OSCA/TMEM63 family of mechanosensitive ion channels. OSCA/TMEM63 proteins constitute a highly conserved family found in all eukaryotic kingdoms so far investigated (Hou et al., 2014; Yuan et al., 2014; Murthy et al., 2018; Wu et al., 2022). The family designation derives from the names of the major representatives in plants (CSC1/OSCA) and animals (TMEM63), respectively. Genomes of fungi, plants, and animals encode multiple OSCA/TMEM63 proteins (Edel and Kudla, 2015), a small number of which have been localized to specific cell membranes and/or have been experimentally shown to be associated with specific physiological processes. For example, in *Penicillium chrysogenum* PenV (UniProt B6HTR9) is localized to the vacuolar membrane, where it plays an essential role in β-lactam synthesis (Fernández-Aguado et al., 2013; Martín and Liras, 2021). As another example, *Schizosaccharomyces pombe* Rsn1 (UniProt O43022) is a plasma membrane protein localizing to expanding cell tips and septation sites (Matsuyama et al., 2006).

The structures of *Arabidopsis thaliana* OSCA1.1 (Zhang et al., 2018) and OSCA1.2 (Jojoa-Cruz et al., 2018; Liu et al., 2018; Maity et al., 2019) have been solved via cryo-electron microscopy. Each consists of eleven transmembrane (TM) helices organized into two transmembrane domains (the *N*-terminal RSN1_TM and the centrally located RSN1_7TM domain), plus a major cytosolic domain (PHM7) located between the two transmembrane domains and a further cytosolic region at the *C*-terminus. The proteins' functional state consists

of a symmetric homodimer, whose association is mediated by interactions between the PHM7 cytosolic domains of each subunit (Liu et al., 2018; Zhang et al., 2018; Maity et al., 2019).

All functionally characterized OSCA/TMEM63 proteins act as mechanosensitive ion channels, having effects upon the level of cytosolic calcium ions (Hou et al., 2014; Yuan et al., 2014; Zhao et al., 2016, Jojoa-Cruz et al., 2018; Murthy et al., 2018). This includes the sole functionally characterized family member amongst the fungi, Csc1p (UniProt Q06538) of *Saccharomyces cerevisiae*, which was shown to function as an osmotically gated calcium conductance channel when heterologously expressed in a Chinese hamster ovary cell line (Hou et al., 2014).

Calcium ions serve as important second messengers in all eukaryotic cells (Luan and Wang, 2021), acting in processes whereby localized changes in the concentration of cytosolic Ca^{2+} serve to regulate the activity of a range of specialized calcium-binding proteins. Cytosolic Ca^{2+} concentrations are governed by integrated systems of sensors, pumps, and ion channels, the activities of which are in turn regulated by a variety of intracellular and extracellular factors (Case et al., 2007; Clapham, 2007). Mechanosensitive ion channels, including OSCA/TMEM63 proteins, are those channels whose permeability changes as a function of physical stresses exerted upon the membrane (Jin et al., 2020), such as would result from changes in turgor pressure or, in the case of walled cells, changes in the cell wall's capacity to resist turgor (Hamilton et al., 2015).

Calcium ion signaling plays a key role in regulating several physiological and morphogenetic processes in fungi. One of the best characterized examples is a cell wall maintenance process in *S. cerevisiae*, in which a mechanosensitive plasma membrane Ca^{2+} channel consisting of Mid1 and Cch1 (both in protein families different from OSCA/TMEM63

proteins) transduces topological changes in the plasma membrane into a cytosolic calcium pulse that triggers a pathway involving the calcineurin complex, which in turn initiates transcription of wall synthesis/repair genes (reviewed in Mishra et al., 2021 and Yang et al., 2022). Orthologues of Mid1 and Cch1 in filamentous fungi have been shown to be involved in growth and virulence of *A. fumigatus* (de Castro et al., 2014), and deletion of CchA and MidA in *A. nidulans* affected hyphal polarity and wall composition (Wang et al., 2012). Takeshita et al. (2017) elegantly demonstrated that MidA and CchA are necessary for the pulsed calcium influxes observed in growing hyphal tips of *A. nidulans* and that the cellular process immediately regulated by these pulses is the exocytosis of apical secretory vesicles, with direct effects upon the rate of growth of hyphal tips and on hyphal morphology. Studies such as these confirm that mechanosensitive calcium channels, as a general functional class, play a role in morphogenesis and cell wall maintenance in filamentous fungi, though to date we are unaware of studies implicating OSCA/TMEM63 proteins in either process.

2. Materials and methods

2.1 Strains, media, and culture methods

Strains used in this study are listed in Table 1. Formulations of minimal medium (MM) and complete medium (CM) are described in Hill et al. (2006). Cell wall inhibiting agents Calcofluor White (CFW; Blankophor BBH) and Congo Red (CR) were added to MM agar using stock solutions consisting of 10 mg/ml in 25 mM KOH (CFW) and 10 mg/ml (CR, aq.). BAPTA and EGTA were added to MM agar medium using stock solutions of 250 mM in DMSO and 500 mM (aq. pH 6.5), respectively. All experimental controls were carried out with the appropriate concentrations of solvent alone. Unless otherwise specified, cultures were incubated at 30°C.

1 CFW was a gift from Bayer AG. All other biochemicals were purchased from Sigma-Aldrich
2 Chemical Company (St. Louis, MO, USA).

3 *2.2 Library transformations and identification of complementing genes*

4 Prior work in our lab identified strain ts1-49 (Harris et al., 1994) as a CFW-
5 hypersensitive strain during a screen for mutations in genes involved in regulating cell wall
6 synthesis and integrity. The mutation in ts1-49 was designated *calF*7 (Hill et al., 2006). Strain
7 ts1-49 was then crossed to strain GR5 (A773; Fungal Genetics Stock Center; FGSC; McCluskey
8 et al., 2010) to generate a pyrimidine-auxotrophic mutant strain (R191) capable of being
9 transformed with the AMA-NotI genomic library (Osherov et al., 2000; FGSC) as described by
10 Yelton et al. (1984). Transformed protoplasts exhibiting restoration of pyrimidine prototrophy
11 were selected on minimal medium containing 1.1 M sorbitol, and conidia from transformed
12 colonies were tested for restoration of wildtype resistance to CFW. Two *calF*7-complemented
13 strains were selected for further study.

14 Total DNA was isolated from each complemented strain using standard methods, and
15 plasmids were recovered by transforming competent *E. coli*. Two plasmids (designated pR191-
16 XF2 and pR191-XF7) complemented the *calF*7 phenotype upon retransformation of strain
17 R191. The genomic inserts of the plasmids were end-sequenced using vector-specific primers
18 (Park and Yu, 2012; primers used in this study are listed in Supplementary Table 1), and the
19 resulting sequences were compared to the Broad Institute *Aspergillus nidulans* sequenced DNA
20 database (then curated by the *Aspergillus* Sequencing Project, Broad Institute of MIT and
21 Harvard; Galagan et al., 2005) to identify the complementing sequences. Gene AN2880 was
22 found to be present in the insert of both complementing plasmids.

23 *2.3 Cloning of AN2880*

1 AN2880 was PCR-amplified from both strain A28 (wild type) and strain ts1-49 (*calF*7
2 mutant) genomic DNA with an additional 536 base pairs of upstream sequence and 533 base
3 pairs of downstream sequence, using *Pfu* Turbo® polymerase (Agilent Technologies) and gene-
4 specific primers containing five-prime extensions encoding restriction sites for
5 *Kpn*I. Restriction-digested PCR products were ligated into the pRG3-AMA1-NotI plasmid
6 (FGSC), using Quick Ligation™ enzyme (New England Biolabs). The constructs containing
7 wild type and mutant-strain AN2880 (copied from A28 and ts1-49, respectively) were used to
8 transform protoplasts from *calF*7 strain R191, and pyrimidine-prototrophic transformants
9 (designated R394 and R395, respectively) were tested for complementation of the *calF*7
10 phenotype.

11 *2.4 Sequencing the mutant strain allele*

12 The AN2880 ORF of mutant strain ts1-49 was PCR amplified from genomic DNA using
13 the same primers used in the preceding section and PfuTurbo® polymerase. Two separate PCR
14 reactions were run, and products from each reaction were cloned into pGEM-5Zf(+) (Promega
15 Corp.) before transformation of competent *E. coli*. Two clones from each PCR reaction were
16 selected for sequencing using overlapping primer sets (not listed) giving at least 2-fold coverage
17 of each sequence. To identify the genetic lesion in AN2880, the respective sequences were
18 aligned to the wild type (strain A4) genomic DNA sequence available through the Broad Institute
19 *Aspergillus nidulans* sequenced DNA database and to our own sequencing of the identical region
20 of strain GR5 (parent strain of strain R191) using Clustal Omega (Madeira et al., 2022).

21 *2.5 Domain and Feature Analysis*

22 Putative protein domains were identified using the Pfam domain prediction program
23 InterPro (https://www.ebi.ac.uk/interpro/; Paysan-Lafosse et al., 2022). All domain and motif

predictions were further checked using Clustal Omega to align the predicted AN2880 gene product to well-characterized SwissProt orthologues from the yeasts *S. cerevisiae* (Csc1p, Q06538) and *S. pombe* (Rsn1, O43022), as well as to PenV (B6HTR9) from the filamentous ascomycete *Penicillium rubens* and a predicted TrEMBL orthologue from the filamentous ascomycete *Neurospora crassa* (Q7S914). A graphical display of domain conservation amongst representative OSCA/TMEM63 proteins is shown in Supplementary Figure 1.

2.6 Modeling of CalF^{WT} and CalF^{G638R} upon S. pombe C354.08c

Using AlphaFold (Jumper et al., 2021; Varadi et al., 2021), the *S. pombe* C354.08c OSCA homologue (AlphaFold model AF-O43022-F1 from UniProt: O43022) was used as the initial structural template for the native CalF protein. To create the model for CalF^{G638R} the native model was imported into UCSF Chimera (Pettersen et al., 2004), and a single residue substitution was created at residue G638 using the Rotamers function. The highest probability rotamer from the Dunbrack 2010 library (Shapovalov et al., 2011), which did not cause any steric clashing within the pore was selected as the appropriate rotamer. After the *in-silico* substitution was performed, structural analysis in Chimera was carried out to evaluate the impact of the G638R substitution in CalF.

2.7 Strain construction

Mendelian crosses followed standard genetic procedures for *Aspergillus nidulans* (Käfer, 1977). For strain construction via molecular manipulation (*C*-terminal tagging and gene deletion) linear constructs were created via fusion PCR (Szewczyk et al., 2006), consisting of transforming "cassettes" plus ca. 1-kbp flanking segments of genomic DNA which target the cassettes to intended integration sites. Phusion® High-Fidelity DNA Polymerase (New England Biolabs) was used in generating all PCR products, which were then purified using the Qiagen

PCR purification kit (Qiagen Inc.). For *C*-terminal GFP, mRFP, and tdTomato tagging, GA5::*GFP*::*AfpyrG* , GA5::*mRFP*::*AfpyrG*, and GA5::*tdTomato::AfpyrG* cassettes were PCR-amplified using plasmids pFNO3, pXDRFP4, and pYX2, respectively, as templates. pFNO3 and pXDRFP4 (Yang et al., 2004) were obtained from FGSC. pYX2 was a gift from Berl Oakley (The University of Kansas). For gene deletions, the *Aspergillus fumigatus riboB* gene (Afu1g13300) was ligated to sequences corresponding to ca. 1 kbp on either side of the coding regions of the genes to be deleted. Recipient strains were transformed according to Osmani *et al*. (2006). Unless otherwise indicated, the *nkuA* deletion strain A1145 (FGSC) served as the recipient. Deletions were confirmed by PCR.

2.7. Microscopy

All microscopy observations were made using hyphae growing on the surface of solid media. Fluorescence observations were made with an Olympus BF53F epifluorescence microscope equipped with a 1.30 numerical aperture 100× oil immersion objective, an Olympus DP80 Dual CCD camera, a pE-300 LED illuminator (CoolLED, Andover, UK), and Olympus cellSens® operating software. Fluorescence observations employed filter sets 39002-BX3 (excitation 480 nm, dichroic 505 nm, emission 535 nm) and 39010-BX3 (excitation 560 nm, dichroic 600, emission 635 nm) for imaging of GFP and mRFP/tdTomato, fluorescence channels, respectively.

3. Results

3.1 Mutant phenotype and identification of the mutated gene

Strains bearing the *calF*7 mutation are hypersensitive to agents imposing cell wall stress (Figure 1A). We were able to complement the hypersensitivity phenotype of *calF*7 strain R191

with either of two plasmids (designated XF2 and XF7) isolated during a genomic library screen, each of which contained a full-length copy of gene AN2880. AN2880 copied from wild type strain A28 also complemented the phenotype, but AN2880 from *calF*7 strain R1-49 did not (Figure 1B). Deletion of AN2880 replicates the CFW-hypersensitive *calF*7 phenotype (Figure 1C), while colony growth and conidiation remain indistinguishable from wild type.

According to the FungiDB database (https://fungidb.org/fungidb/app/; Amos et al., 2021), AN2880 is located on chromosome VI at position A4:2511792..2514883(- strand). Attempts to map the *calF*7 phenotype to this region of chromosome VI using meiotic mapping strains (FGSC) were inconclusive. Therefore, a cross was made between strain R1843 (expressing the GFP-tagged product of AN2880) and AN2880 deletion strain R1860, and the resulting progeny were assessed for both phenotypes. Out of 150 progeny strains examined, zero percent showed recombination between the two phenotypes, which is consistent with location of the *calF*7 mutation in AN2880. We therefore use *calF* as an alternative name for gene AN2880.

Sequencing of AN2880 from *calF*7 strain R191 revealed a G-to-C transversion at base pair 2015 (base pair 1912 after removing introns) within the 3092-bp long coding region. This mutation is predicted to result in a glycine-to-arginine substitution at position 638 of the predicted 945-residue gene product (https://fungidb.org/fungidb/app/), which is listed at UniProt under accession number Q5B9A0. As shown in Figure 2A, the predicted G638R substitution occurs in a region strongly conserved within orthologues of filamentous fungi from all major terrestrial phyla, as well as in *Schizosaccharomyces pombe* and some members of Chyridiomycota. This residue and its surrounding context are not, however, conserved in members of class Saccharomycetes, such as *Saccharomyces cerevisiae* and *Candida albicans*.

3.2 Domain and Feature Analysis

Based on the experimentally demonstrated structure (Zhang et al., 2018) of *Arabidopsis thaliana* orthologue OSCA1 (UniProt Q9XEA1; 22% identity; 43% positives; E = 1e-37), CalF is a multi-pass transmembrane protein having three functional domains (RSN1_TM, PHM7_cyt, and RSN1_7TM) with a membrane topology as shown in Figures 2B and 2C. The G638R substitution lies within a cytosolic-face loop located between helix #9 and helix #10 of domain RSN1_7TM (Figures 2C and 2D).

Both the wild type G638 and the mutant G638R homology models predict the presence of a transmembrane pore in the RSN1_7TM domain and place the loop containing residue 638 at the cytosolic-face opening of that pore (Figure 2E). The majority of the residues defining the loop and the pore were modeled at a confidence level greater than 90%, and the Ramachandran plot analyses for the native G638 and the G638R variants demonstrated that all residues defining the pore were in allowable structural regions. Our model predicts that in the native protein the small glycine residue does not intrude into the pore space, leaving a pore diameter at the cytosolic face of approximately 8.6Å (left-hand panels in Figure 2E), measured using the distance between the side chains of S637 to A356 as a measure of minimal pore diameter. However, in the G638R variant the arginine side chain is predicted to intrude into the pore opening, resulting in a pore diameter of only 4.2Å (right-hand panels in Figure 2E). The predicted channel spaces provided by the respective protein models are graphically compared to the size of a solvated Ca^{2+} ion (diameter 6.7Å; Barger and Dillon, 2016).

3.3 Subcellular Localization

As shown in Figure 3, the *C*-terminally tagged wild-type *calF* gene product (CalF::GFP) localizes both to hyphal tips and to sites of septum formation. The principal apical signal is found in the Spitzenkörper (Spk), as demonstrated by its colocalization with a tdTomato-tagged

construct of the Spk-resident formin SepA (Sharpless and Harris, 2002) and to the tip-most ca. 5 to 8 micrometers of the apical cell plasma membrane (panels 3A – 3C). A less intense signal can also be seen in unidentified cytoplasmic compartments of the apical cell (panel 3A and inset).

At septation sites, the CalF::GFP signal is first detectable as a peripheral ring forming at the same location at which initial coalescence of the contractile actomyosin ring (CAR) occurs in the cell cortex (panels 3D – 3F). Though the CalF signal overlaps with signals of CAR components such as actin or the formin SepA prior to onset of CAR ingression, the CalF signal is only partially congruent with the distribution of CAR components during ingression (panels 3G – 3I). Specifically, CalF localizes not just to the advancing margin of the septal membrane (at which site CAR components are also localized), but also to the entire invaginated portion of the septal plasma membrane. CalF remains associated with the septal membrane during the entire period of CAR ingression, but the signal is no longer present after CAR dispersal. As shown in panels 3J – 3L, except where septa are forming, plasma membranes of subapical compartments (labeled by the broadly distributed plasma membrane protein MtlA::mRFP; Futagami et al., 2014) lack the CalF signal entirely.

3.4 Requirement of Extracellular Calcium Ion for Tolerance of Wall Stress

Because several AN2880 orthologues in animals and plants have been experimentally shown to function as mechanosensitive calcium ion channels (e.g., Hou et al., 2014), we investigated whether we could detect any degree of Ca^{2+} dependence regarding hypersensitivity to CFW or Congo Red. As shown in Figure 4A, addition of 120 mM $CaCl_2$ to minimal medium confers upon *calF*7 and AN2880-deletion strains near-wild-type levels of tolerance to CFW and CR. Supplementing media with equimolar concentrations of $MgCl_2$ produced no beneficial effect on CFW tolerance, indicating that $CaCl_2$-induced tolerance is not due simply to osmotic

stabilization. Correspondingly, chelation of basal levels of calcium ions in minimal medium by including either 5 mM EGTA or 5 mM BAPTA in the medium essentially abolishes the ability of wild type strain A28 to tolerate CFW or CR (Figure 4B). Together, these observations support the conclusion that tolerance to these particular wall-compromising agents is at least partly dependent upon the pool of extracellular calcium ions.

4. Discussion

The most distinctive aspect of the *calF*7 phenotype is its hypersensitivity to the cell wall damaging agents Calcofluor White and Congo Red. Both chemicals bind to β-glycan polymers, interfering with the inter-chain hydrogen bonding necessary for the crystallization step of microfibril assembly in growing walls (Maeda and Ishida, 1967; Wood, 1980). Hypersensitivity to these agents is well established as an indicator of defects in cell wall integrity in yeasts (e.g., Ram et al., 1994) and filamentous fungi (e.g., Hill et al., 2006), as well as defects in formation of septa which are necessary to prevent damage control in the face of wall-perturbing compounds (Spence et al., 2022).

The results of this investigation indicate that the *calF*7 mutation resides in a gene encoding a protein in the OSCA/TMEM63 family of mechanosensitive calcium transport proteins. The properties of the family show a high degree of evolutionary conservation (Jin et al., 2020; Miles et al., 2022). CalF localizes principally to two plasma membrane domains, each of which is associated with cell wall synthesis: the growing hyphal apex and sites of septum formation. Since the Spitzenkörper (Spk) is understood to be a site at which secretory vesicles become concentrated prior to their ultimate dispatch to the growing hyphal apex (Bartnicki-Garcia et al., 1995; Takeshita et al., 2018; Higuchi et al., 2021, Pinar and Peñalva, 2021), the

strong association of CalF with the Spk need not be seen as indicating that its function is necessarily played out in this location. The distribution of CalF in the apical cell bears a strong resemblance to the distribution of ChsB, which cycles between the plasma membrane and the trans-Golgi network (TGN) via endocytosis at the endocytic collar with subsequent re-delivery to the Spk and the plasma membrane (Hernández-González et al., 2018). This suggests the strong likelihood that the plasma membrane distribution of CalF in the apical compartment is maintained by the same mechanism, in which case CalF-containing cytoplasmic compartments are the TGN. Similarly, endocytosis during later stages of septum formation (reviewed by Mouriño-Pérez, 2013) is a probable mechanism for the eventual disappearance of CalF from completed septa.

We are aware of only one other fungal OSCA/TMEM63 protein having a plasma membrane distribution associated with sites of wall synthesis: *S. pombe* rsn1 (SPBC354.08c on PomBase) is reported by Matsuyama et al. (2006) to localize as cytoplasmic dots at the cell tip and sites of septum formation. No growth or septation phenotype has been associated with defects in this locus, however (Hayles et al., 2013).

Despite the close association of CalF with sites of ongoing cell wall synthesis, neither the *calF*7 mutation nor deletion of AN2880 results in observable defects in hyphal morphology, growth rate, or cytokinesis under normal growth conditions. It is reasonable to conclude, therefore, that CalF plays no role (or plays only a non-essential role) during normal growth and cell division, but that its localization at sites of wall synthesis is somehow essential for mounting an effective response against significant threats to wall integrity.

A possible role for CalF in the response to wall compromising agents is shown by the fact that increasing the level of calcium ions in the medium overcomes the CFW-hypersensitive

phenotype of *calF*7 and AN2880 deletion strains, while at the same time depletion of extracellular calcium ions by EGTA or BAPTA impairs the ability of wild type strains to resist CFW. Clearly, the availability of a sufficiently high concentration of extracellular calcium ions plays a role in wild type tolerance to CFW and CR. Thus, we suggest that the hypersensitivity of *calF*7 and AN2880-deletion strains to these agents is related to having access to extracellular calcium ion pools.

A similar demonstration of the requirement of a pool of extracellular Ca^{2+} for wild type resistance to wall stressors was made by Wang et al. (2021), who showed that sensitivity of *A. nidulans* to CFW and CR was increased in strains deleted for the TRP-like calcium channel orthologue *trpR*, and that the inhibitory effect could be lessened by an increased level of calcium ion in the medium. Additionally, Liu et al. (2020) showed that deletion of the mechanosensitive calcium channel components MidA or CchA in *A. niger* resulted in increased sensitivity to CFW and CR. It is important to note, however, that these proteins are all members of families other than OSCA/TMEM63. Thus, a variety of calcium ion channel proteins appear to play roles in the cell's response to wall compromising chemicals in filamentous fungi.

Though OSCA/TMEM63 encoding genes are abundant in the genomes of filamentous fungi, few have been investigated, and none of those so far described has been shown to colocalize with processes of wall synthesis. Nor have any been shown to function in processes of cell wall repair. Included in this brief list of functionally investigated OSCA/TMEM63 proteins in filamentous fungi is PenV in *Penicillium chrysogenum*, which localizes to the vacuolar membrane where it plays an essential role in beta lactam synthesis (Fernández-Aguado et al., 2013; Martín and Liras, 2021). In *Candida albicans*, deletion of either orf19.4805 (encoding a protein with UniProt accession number A0A1D8PEK8) or the gene encoding

1 CaPhm7 (Jiang and Pan, 2018; Jiang and Yang, 2018) resulted in elevated sensitivity to the
2 membrane-compromising agents SDS and ketoconazole, but no investigation of sensitivity to
3 wall compromising agents was reported.

4 The mutation identified in the *calF*7 allele is predicted to cause a glycine-to-arginine
5 (neutral to charged) amino acid substitution within a short cytosolic domain located between the
6 ninth and tenth transmembrane helices of the highly conserved RSN1_7TM domain (formerly
7 called the DUF221 domain – PF02714), within which lies the protein's ion-permeable pore
8 (Jojoa-Cruz et al., 2018, Zhang et al., 2018). Gly-638 and its surrounding sequence context are
9 well conserved amongst the members of the major terrestrial fungal phyla (Ascomycota,
10 Basidiomycota, and Mucoromycota). The principal exception occurs among members of the
11 ascomycete subphylum Saccharomycotina in which the context is conserved, but the residue
12 homologous to *A. nidulans* G638 is typically a different amino acid.

13 Although residue 638 lies within a cytosolic loop and not within one of the
14 transmembrane helices that define the pore-proper, our modeling places the loop immediately
15 beside the cytosolic opening of the pore. In our model, the ca. 8.6Å pore diameter at the
16 cytosolic face of the native protein opening would be more than enough to accommodate the
17 passing of a solvated Ca^{2+} ion having a diameter of approximately 6.7Å (Barger and Dillon,
18 2016), while the 4.2Å predicted minimum width of the G638R pore opening is well below the
19 diameter of the hydrated ion. If the AN2880 gene product functions as a calcium conductance
20 channel, as do all other functionally characterized OSCA/TMEM63 proteins, then this decrease
21 in pore diameter would greatly impair the channel's ability to allow ions to pass across the
22 membrane.

In summary, we have shown that the ability of *A. nidulans* to deal with cell wall-stressing chemicals such as Calcofluor White and Congo Red depends at least in part upon having access to extracellular pools of calcium ions and that a mutation in a plasma-membrane-localized member of the OSCA/TMEM63 family of mechanosensitive calcium channels results in severely reduced ability to respond to these same stresses. The predicted consequence of the mutation is to structurally occlude the principal conductance pore of the encoded protein. To our knowledge, this is the first member of this protein family shown to play a role in maintenance of cell wall integrity in the filamentous fungi.

Acknowledgments

We thank Berl Oakley and Brian Shaw for sharing strains and plasmids. Support for this work was provided by National Science Foundation Grants NSF grants RUI-1615192 and RUI-2222841 to LJH and TWH, and by the Charles Robertson Fund in support of undergraduate research at Rhodes College.

Appendix A. Supplementary material

Supplementary data associated with this article can be found in the online version at http:

References

Amos, B., Aurrecoechea, C., Barba, M., Barreto, A., Basenko, E.Y., Belnap, R., Blevins, A.S., Böhme, U., Brestelli, J., Brunk, B.P., 2021. VEuPathDB: the eukaryotic pathogen, vector and host bioinformatics resource center. Nucleic Acids Res. 50(D1), D898-D911.

1 Barger, J. P., Dillon, P.F., 2016. Near-membrane electric field calcium ion dehydration. Cell
2 Calcium 60, 415-422.
3 Bartnicki-Garcia, S., Bartnicki, D.D., Gierz, G., López-Franco, R., Bracker, C.E., 1995.
4 Evidence that Spitzenkörper behavior determines the shape of a fungal hypha: a test of the
5 hyphoid model. Exp. Mycol. 19(2), 153-159.
6 Case, R.M., Eisner, D., Gurney, A., Jones, O., Muallem, S., Verkhratsky, A., 2007. Evolution of
7 calcium homeostasis: from birth of the first cell to an omnipresent signalling system. Cell
8 Calcium 42(4-5), 345-350.
9 Clapham, D.E., 2007. Calcium signaling. Cell 131(6), 1047-1058.
10 De Castro, P.A., Chiaratto, J., Winkelströter, L.K., Bom, V.L.P., Ramalho, L.N.Z., Goldman,
11 M.H.S., Brown, N.A., Goldman, G.H., 2014. The involvement of the Mid1/Cch1/Yvc1
12 calcium channels in *Aspergillus fumigatus* virulence. PLoS One 9(8), e103957.
13 Edel, K.H., Kudla, J., 2015. Increasing complexity and versatility: how the calcium signaling
14 toolkit was shaped during plant land colonization. Cell Calcium 57(3), 231-246.
15 Fernández-Aguado, M., Teijeira, F., Martín, J.F., Ullán, R.V., 2013. A vacuolar membrane
16 protein affects drastically the biosynthesis of the ACV tripeptide and the beta-lactam
17 pathway of *Penicillium chrysogenum*. Appl. Microbiol. Biotechnol. 97, 795-808.
18 Futagami, T., Seto, K., Kajiwara, Y., Takashita, H., Omori, T., Takegawa, K., Goto, M., 2014.
19 The putative stress sensor protein MtlA is required for conidia formation, cell wall stress
20 tolerance, and cell wall integrity in *Aspergillus nidulans*. Biosci. Biotechnol. Biochem.
21 78(2), 326-335.
22 Galagan, J.E., Calvo, S.E., Cuomo, C., Ma, L.-J., Wortman, J.R., Batzoglou, S., Lee, S.-I.,
23 Baştürkmen, M., Spevak, C.C., Clutterbuck, J., et al., 2005. Sequencing of *Aspergillus*

1 *nidulans* and comparative analysis with *A. fumigatus* and *A. oryzae*. Nature 438(7071),
2 1105-1115.
3 Hamilton, E.S., Schlegel, A.M., Haswell, E.S., 2015. United in diversity: mechanosensitive ion
4 channels in plants. Annu. Rev. Plant Biol. 66, 113-137.
5 Harris, S.D., Morrell, J.L., Hamer, J.E., 1994. Identification and characterization of *Aspergillus*
6 *nidulans* mutants defective in cytokinesis. Genetics 136(2), 517-532.
7 Hayles, J., Wood, V., Jeffery, L., Hoe, K.-L., Kim, D.-U., Park, H.-O., Salas-Pino, S.,
8 Heichinger, C., Nurse, P., 2013. A genome-wide resource of cell cycle and cell shape
9 genes of fission yeast. Open Biology 3(5), 130053.
10 Hernández-González, M., Bravo-Plaza, I., Pinar, M., de Los Ríos, V., Arst Jr, H.N., Peñalva,
11 M.A., 2018. Endocytic recycling via the TGN underlies the polarized hyphal mode of life.
12 PLoS genetics, 14(4), p.e1007291.
13 Higuchi, Y., 2021. Membrane traffic in *Aspergillus oryzae* and related filamentous fungi. J.
14 Fungi 7(7), 534.
15 Hill, T.W., Loprete, D.M., Momany, M., Ha, Y., Harsch, L.M., Livesay, J.A., Mirchandani, A.,
16 Murdock, J.J., Vaughan, M.J., Watt, M.B., 2006. Isolation of cell wall mutants in
17 *Aspergillus nidulans* by screening for hypersensitivity to Calcofluor White. Mycologia
18 98(3), 399-409.
19 Hou, C., Tian, W., Kleist, T., He, K., Garcia, V., Bai, F., Hao, Y., Luan, S., Li, L., 2014.
20 DUF221 proteins are a family of osmosensitive calcium-permeable cation channels
21 conserved across eukaryotes. Cell Res. 24(5), 632-635.
22 Jiang, L., Pan, H., 2018. Functions of CaPhm7 in the regulation of ion homeostasis, drug
23 tolerance, filamentation and virulence in *Candida albicans*. BMC Microbiol. 18, 1-8.

1 Jiang, L., Yang, Y., 2018. The putative transient receptor potential channel protein encoded by
2 the orf19.4805 gene is involved in cation sensitivity, antifungal tolerance, and
3 filamentation in *Candida albicans*. Can. J. Microbiol. 64(10), 727-731.
4 Jin, P., Jan, L.Y., Jan, Y.-N., 2020. Mechanosensitive ion channels: structural features relevant
5 to mechanotransduction mechanisms. Annu. Rev. Neurosci. 43, 207-229.
6 Jojoa-Cruz, S., Saotome, K., Murthy, S.E., Tsui, C.C.A., Sansom, M.S.P., Patapoutian, A., Ward,
7 A.B., 2018. Cryo-EM structure of the mechanically activated ion channel OSCA1. 2. Elife
8 7, e41845.
9 Jumper, J., Evans, R., Pritzel, A., Green, T., Figurnov, M., Ronneberger, O., Tunyasuvunakool,
10 K., Bates, R., Žídek, A., Potapenko, A., Bridgland, A., Meyer, C., et al., 2021. Highly
11 accurate protein structure prediction with AlphaFold. Nature 596, 583-589.
12 Käfer, E., 1977. Meiotic and mitotic recombination in *Aspergillus* and its chromosomal
13 aberrations. Adv. Genet. 19, 33-131.
14 Liu, L., Yu, B., Sun, W., Liang, C., Ying, H., Zhou, S., Niu, H., Wang, Y., Liu, D., Chen, Y.,
15 2020. Calcineurin signaling pathway influences *Aspergillus niger* biofilm formation by
16 affecting hydrophobicity and cell wall integrity. Biotechnol. Biofuels 13, 1-13.
17 Liu, X., Wang, J., Sun, L., 2018. Structure of the hyperosmolality-gated calcium-permeable
18 channel OSCA1. 2. Nat. Commun. 9(1), 5060.
19 Luan, S., Wang, C., 2021. Calcium signaling mechanisms across kingdoms. Annu. Rev. Cell
20 Dev. Biol. 37, 311-340.
21 Madeira, F., Pearce, M., Tivey, A.R.N., Basutkar, P., Lee, J., Edbali, O., Madhusoodanan, N.,
22 Kolesnikov, A., Lopez, R., 2022. Search and sequence analysis tools services from
23 EMBL-EBI in 2022. Nucleic Acids Res. 50(W1), W276-W279.

1 Maeda, H., Ishida, N., 1967. Specificity of binding of hexopyranosyl polysaccharides with
2 fluorescent brightener. J. Biochem. 62(2), 276-278.
3 Maity, K., Heumann, J.M., McGrath, A.P., Kopcho, N.J., Hsu, P.-K., Lee, C.-W., Mapes, J.H.,
4 Garza, D., Krishnan, S., Morgan, G.P., 2019. Cryo-EM structure of OSCA1. 2 from *Oryza*
5 *sativa* elucidates the mechanical basis of potential membrane hyperosmolality gating.
6 Proc. Natl. Acad. Sci. U.S.A. 116(28), 14309-14318.
7 Martín, J.F., Liras, P., 2021. The PenV vacuolar membrane protein that controls penicillin
8 biosynthesis is a putative member of a subfamily of stress-gated transient receptor calcium
9 channels. Curr. Res. Biotechnol. 3, 317-322.
10 Matsuyama, A., Arai, R., Yashiroda, Y., Shirai, A., Kamata, A., Sekido, S., Kobayashi, Y.,
11 Hashimoto, A., Hamamoto, M., Hiraoka, Y., 2006. ORFeome cloning and global analysis
12 of protein localization in the fission yeast *Schizosaccharomyces pombe*. Nat. Biotechnol.
13 24(7), 841-847.
14 McCluskey, K., Wiest, A., Plamann, M., 2010. The Fungal Genetics Stock Center: a repository
15 for 50 years of fungal genetics research. J. Biosci. 35, 119-126.
16 Miles, L., Powell, J., Kozak, C., Song, Y., 2022. Mechanosensitive ion channels, axonal growth,
17 and regeneration. Neuroscientist 29(4), 421-444.
18 Mishra, R., Minc, N., Peter, M., 2021. Cells under pressure: how yeast cells respond to
19 mechanical forces. Trends Microbiol. 30(5), 495-510.
20 Mouriño-Pérez, R.R., 2013. Septum development in filamentous ascomycetes. Fungal Biol.
21 Rev., 27(1), 1-9.

1 Murthy, S.E., Dubin, A.E., Whitwam, T., Jojoa-Cruz, S., Cahalan, S.M., Mousavi, S.A.R., Ward,
2 A.B., Patapoutian, A., 2018. OSCA/TMEM63 are an evolutionarily conserved family of
3 mechanically activated ion channels. Elife 7, e41844.
4 Osherov, N., Mathew, J., May, G.S., 2000. Polarity-defective mutants of *Aspergillus nidulans*.
5 Fungal Genet. Biol. 31(3), 181-188.
6 Park, H.-S. Yu, J.H., 2012. Multicopy genetic screen in *Aspergillus nidulans*. Methods Mol.
7 Biol. 944, 183-190.
8 Paysan-Lafosse, T., Blum, M., Chuguransky, S., Grego, T., Pinto, B., Salazar, G.A., Bileschi,
9 M.L., Bork, P., Bridge, A., Colwell, L., 2023. InterPro in 2022. Nucleic Acids Res.
10 51(D1), D418-D427.
11 Pettersen, E.F., Goddard T.D., Huang C.C., Couch G.S., Greenblatt D.M., Meng E.C., Ferrin
12 T.E., 2004. UCSF Chimera –visualization system for exploratory research and analysis. J.
13 Comput. Chem. Oct;25(13), 1605-12.
14 Pinar, M., Peñalva, M.A., 2021. The fungal RABOME: RAB GTPases acting in the endocytic
15 and exocytic pathways of *Aspergillus nidulans* (with excursions to other filamentous
16 fungi). Molec. Microbiol. Jul;116(1), 53-70.
17 Ram, A.F.J., Wolters, A., Hoopen, R.T., Klis, F.M., 1994. A new approach for isolating cell
18 wall mutants in *Saccharomyces cerevisiae* by screening for hypersensitivity to calcofluor
19 white. Yeast 10(8), 1019-1030.
20 Shapovalov, M.S., Dunbrack, R.L., Jr., 2011. A Smoothed backbone-dependent rotamer library
21 for proteins derived from adaptive kernel density estimates and regressions. Structure, 19,
22 844-858.

1 Sharpless, K.E., Harris, S.D., 2002. Functional characterization and localization of the
2 *Aspergillus nidulans* formin SEPA. Molec. Biol. Cell 13, 469-479.
3 Varadi, M., Anyango, S., Deshpande, M., Nair, S., Natassia, C., Yordanova, G., Yuan, D., Stroe,
4 O., Wood, G., Laydon, A., Žídek, A., Green, T., Tunyasuvunakool, K., et. al., 2021.
5 AlphaFold Protein Structure Database: massively expanding the structural coverage of
6 protein-sequence space with high-accuracy models. Nucleic Acids Res. 50(D1), D439–
7 D444.
8 Spence, R.N., Huso, W., Edwards, H., Doan, A., Reese, S., Harris, S.D., Srivastava, R., Marten,
9 M.R., 2022. *Aspergillus nidulans* septa are indispensable for surviving cell wall stress.
10 Microbiol. Spectr. 10(1), e02063-21.
11 Szewczyk, E., Nayak, T., Oakley, C.E., Edgerton, H., Xiong, Y., Taheri-Talesh, N., Osmani,
12 S.A., Oakley, B.R., 2006. Fusion PCR and gene targeting in *Aspergillus nidulans*. Nat.
13 Protoc. 1(6), 3111-3120.
14 Takeshita, N., Evangelinos, M., Zhou, L., Serizawa, T., Somera-Fajardo, R.A., Lu, L., Takaya,
15 N., Nienhaus, G.U., Fischer, R., 2017. Pulses of Ca^{2+} coordinate actin assembly and
16 exocytosis for stepwise cell extension. Proc. Natl. Acad. Sci. U.S.A. 114(22), 5701-5706.
17 Takeshita, N., 2018. Oscillatory fungal cell growth. Fungal Genet. Biol. 110, 10-14.
18 Wang, H., Chen, Q., Zhang, S., Lu, L., 2021. A transient receptor potential-like calcium ion
19 channel in the filamentous fungus *Aspergillus nidulans*. J. Fungi 7(11), 920.
20 Wang, S., Cao, J., Liu, X., Hu, H., Shi, J., Zhang, S., Keller, N.P., Lu, L., 2012. Putative
21 calcium channels CchA and MidA play the important roles in conidiation, hyphal polarity
22 and cell wall components in *Aspergillus nidulans*. PLoS One 7(10):e46564.

1 Wood, P.J., 1980. Specificity in the interaction of direct dyes with polysaccharides. Carbohydr.
2 Res 85(2), 271-287.
3 Wu, X., Yuan, F., Wang, X., Zhu, S., Pei, Z.M., 2022. Evolution of osmosensing OSCA1 Ca^{2+}
4 channel family coincident with plant transition from water to land. Plant Genome 15(2),
5 e20198.
6 Yang, Y., Xie, P., Li, Y., Bi, Y., Prusky, D.B., 2022. Updating insights into the regulatory
7 mechanisms of calcineurin-activated transcription factor Crz1 in pathogenic fungi. J. Fungi
8 8(10), 1082.
9 Yelton, M.M., Hamer, J.E., Timberlake, W.E., 1984. Transformation of *Aspergillus nidulans* by
10 using a trpC plasmid. Proc. Natl. Acad. Sci. U.S.A. 81(5), 1470-1474.
11 Yuan, F., Yang, H., Xue, Y., Kong, D., Ye, R., Li, C., Zhang, J., Theprungsirikul, L., Shrift, T.,
12 Krichilsky, B., 2014. OSCA1 mediates osmotic-stress-evoked Ca^{2+} increases vital for
13 osmosensing in *Arabidopsis*. Nature 514(7522), 367-371.
14 Zhang, M., Wang, D., Kang, Y., Wu, J.-X., Yao, F., Pan, C., Yan, Z., Song, C., Chen, L., 2018.
15 Structure of the mechanosensitive OSCA channels. Nat. Struct. Mol. Biol. 25(9), 850-858.
16 Zhao, X., Yan, X., Liu, Y., Zhang, P., Ni, X., 2016. Co-expression of mouse TMEM63A,
17 TMEM63B and TMEM63C confers hyperosmolarity activated ion currents in HEK293
18 cells. Cell Biochem. Funct. 34(4), 238-24.
19

20 **Figure Legends**

21 Figure 1. The *calF*7 mutation results in hypersensitivity to Calcofluor White (CFW), which can
22 be complemented by the wild type allele of AN2880. A. Strains A28 and GR5 show wild type
23 resistance to CFW. Strains ts1-49 and R191 bear the *calF*7 mutation. Strains XF2 and XF7

1 resulted from transformation of R191 with separate gDNA library plasmids containing full-
2 length copies of gene AN2880. Strains were inoculated using toothpick samples from
3 conidiating colonies of the respective cultures and grown for three days at 30°C. B. Wild type
4 AN2880 complements the *calF*7 phenotype, but AN2880 copied from a *calF*7 strain does not.
5 WT = strain GR5 (parent of strain R191); *calF*7 = strain R191; $AN2880^{A28}$ = strain R191
6 transformed with pRG3 containing AN2880 copied from wild type strain A28; $AN2880^{ts1-49}$ =
7 strain R191 transformed with containing AN2880 copied from *calF*7 strain ts1-49. Strains were
8 inoculated in droplets containing 10,000 conidia onto minimal medium (MM) with or without 4
9 µg/ml CFW. Growth after two days at 30°C is depicted. C. Deletion of AN2880 results in
10 hypersensitivity to Calcofluor White (CFW) and Congo Red (CR). WT= wild type strain A28;
11 Δ*calF* = AN2880 deletion strain R1860. Strains were inoculated in droplets containing 10,000
12 conidia onto minimal medium (MM) with or without 4 µg/ml CFW or 50 µg/ml CR and grown
13 for 3 days at 30°C.
14
15 Figure 2. A. Partial alignment of CalF to selected fungal orthologues. The amino acid change
16 predicted to result from the *calF*7 mutation is a G-to-R substitution at residue 638, highlighted in
17 red. The aligned sequences comprise a portion of the RSN1_7TM domain, demonstrating a high
18 degree of conservation across a wide range of fungal phyla. Depicted orthologues with UniProt
19 accession numbers are *Mucor circinelloides* S2JFV4 (Mucoromycota), *Phanerochaete carnosa*
20 K5W2P2 (Basidiomycota), *Spizellomyces punctatus* A0A0L0HE86 (Chytridiomycota) ,
21 *Schizosaccharomyces pombe* O43022 (Ascomycota), and *Neurospora crassa* Q7S914
22 (Ascomycota). B. Proposed domain structure of CalF. Boundaries of the RSN1_TM,
23 PHM7_cyt, and RSN1_7TM domains are those recognized by Pfam. The position of the G638R

1 substitution is indicated in red. The domain diagram was created using DOG freeware
2 (http://dog.biocuckoo.org/down.php). C. Proposed membrane topology of CalF; color coding
3 corresponds to domain structure in B. D. Detail of the cytosolic loop between helixes 9 and 10,
4 highlighting the position of the G638R substitution. The topology diagrams in C and D were
5 created using Protter (http://wlab.ethz.ch/protter/start/). E. Homology models of the Ca^{2+} ion
6 conductance pore of native and mutated CalF. The pore is viewed from the perspective of the
7 cytosolic face. In all images, the solvated Ca^{2+} ion is depicted as a green sphere. Left-hand
8 panels depict the homology model of the Ca^{2+} ion conductance pore of wild type CalF. The
9 predicted surface through which a diffusing ion would pass is colored coral. In the upper-left
10 panel the surface has been rendered transparent in the immediate region of G638 in order to
11 show its location beneath the modeled surface. The ribbon area colored blue is residue G638.
12 The right-hand panels depict the predicted surface (colored purple) of the G638R *calF*7 gene
13 product. In the upper-right panel the surface has been rendered transparent in the immediate
14 region of R638 in order to show its location beneath the modeled surface. The ribbon area
15 colored blue is residue R638.
16
17 Figure 3. CalF localizes principally to the Spitzenkörper, the apical cell plasma membrane, and
18 the plasma membranes of forming septa. Panels A – C (strain R2713) demonstrate
19 colocalization of CalF::GFP (panel A) with SepA::tdTomato in the Spitzenkörper (panel B);
20 panel C is a merged image of panels A and B. The inset in panel A adjusts CalF signal intensity
21 and contrast to demonstrate more clearly the additional localization in unidentified cytoplasmic
22 compartments, as well as restriction of the plasma membrane signal mainly to the tip-most 5 – 8
23 μm of the cell. Panels D – F (strain R2088) demonstrate colocalization of CalF::GFP (panel D)

with actin (panel E, visualized with Lifeact::mRFP) at the site of initial CAR coalescence. Panel F is a merged image of panels D and E. Panels G – I (strain R2713) demonstrate that CalF::GFP (panel G) is associated with the established region of the maturing septal membrane and not with components of the constricting CAR, represented by SepA::tdTomato (panel H). Panel I is a merged image of panels G and H. Panels J – L (strain R305) demonstrate that CalF::GFP (panel J) is associated with the ingressing septal membrane only during septum formation, but not with the membrane of matured septa. In panel K the plasma membranes of two hyphae are labeled by MtlA::mRFP; CalF colocalizes only with the membrane of the forming septum to the right of the image. Panel L is a merged image of panels J and K. Cultures were grown overnight at 30°C on minimal medium containing appropriate nutritional supplements. Scale bars represent 5 µm.

Figure 4. A. Increasing the level of calcium ion in minimal medium allows *calF*7 and *calF* deletion strains to resist wall-stressing agents. Isosmotic levels of $MgCl_2$ do not improve resistance. WT = strain A28; Δ*calF* = strain R1860; *calF*7 = strain R191. CFW and CR were used at 10 mg/ml; $CaCl_2$ and $MgCl_2$ were used at 120 mM in minimal medium. Inocula consisted of 10,000 conidia in 5-µl drops. Photographs were taken after 3 days at 30°C. B. Addition of calcium ion chelators EGTA or BAPTA to minimal medium reduces the ability of wild type *A. nidulans* to resist Calcofluor White (CFW). Each vertical column represents a progressive two-fold dilution series of strain A28 beginning (top) with 10,000 conidia in 5-µl drops. Control = minimal medium with no additions. CFW was used at 10 mg/ml. EGTA (aq.) and BAPTA (in DMSO) were added at 5 mM. The DMSO concentration in the BAPTA treatment and the BAPTA control was 1.6 %. Photographs were taken after 2 days at 30°C.

Table 1. *Aspergillus nidulans* strains used in this study.

Strain	Genotype	Source
A28	*biA*1; *pabaA*6	FGSC
A1145	*pyrG*89; *nkuA::argB*; *pyroA*4; *riboB*2	FGSC
GR5	*pyrG*89, *wA*3; *pyroA*4	FGSC
ts1-49	*biA*1; *calF*7, *pabaA*6	FGSC
R191	*pyrG*89, *wA*3; *pyroA*4; *calF*7	Hill et al., 2006
R305	*mtlA::mRFP*; *pyroA*4; *calF*::GFP	This study
R394	*pyrG*89*, wA*3; *pyroA*4; *calF*7; *[AN2880^{A28}::pyr-4]*	This study
R395	*pyrG*89*, wA*3; *pyroA*4; *calF*7; *[AN2880^{ts1-49}::pyr-4]*	This study
R1843	*pyroA*4; *CalF::GFP*; *riboB*2	This study
R1860	*pyrG*89, *pabaA*1; Δ*calF::AfRiboB*	This study
R2088	*CalF::GFP*; *riboB*2; *AfpyrG::niiA(p)::Lifeact::mRFP*	This study
R2713	*SepA::tdTomato*; *argB*2*; CalF::GFP*	This study

Constructs enclosed by square brackets were introduced as components of ectopic plasmids. *Af* designations refer to *Aspergillus fumigatus* orthologues. FGSC = Fungal Genetics Stock Center, Kansas State University (McCluskey et al., 2010). Strain ts1-49 comes from the Steven Harris *A. nidulans* temperature-sensitive mutant collection at FGSC. Strain R2088 was created via Mendelian crosses using Lifeact::mRFP-expressing parent strain LQR3, generously provided by Brian Shaw, Texas A&M University.

1
2

Figure 1

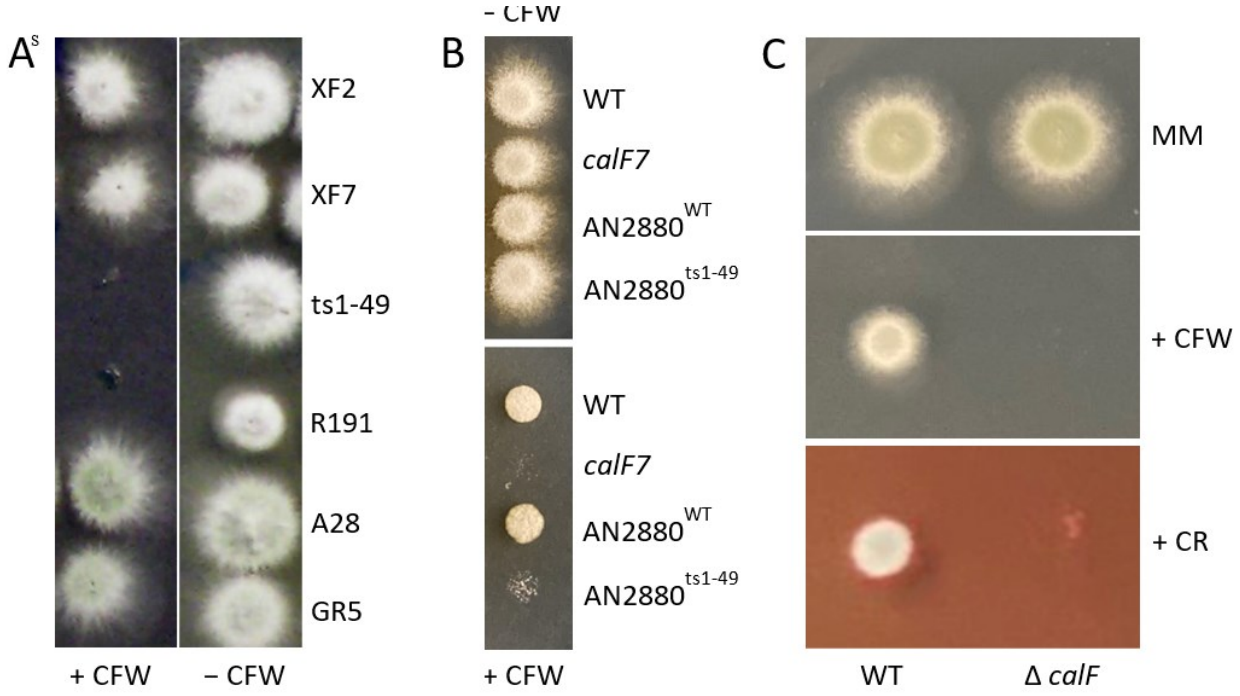
A
XF2
XF7
ts1-49
R191
A28
GR5
+ CFW
− CFW
B
− CFW
WT
calF7
AN2880WT
AN2880ts1-49
WT
calF7
AN2880WT
AN2880ts1-49
+ CFW
C
MM
+ CFW
+ CR
WT
Δ calF

1
2

Figure 2

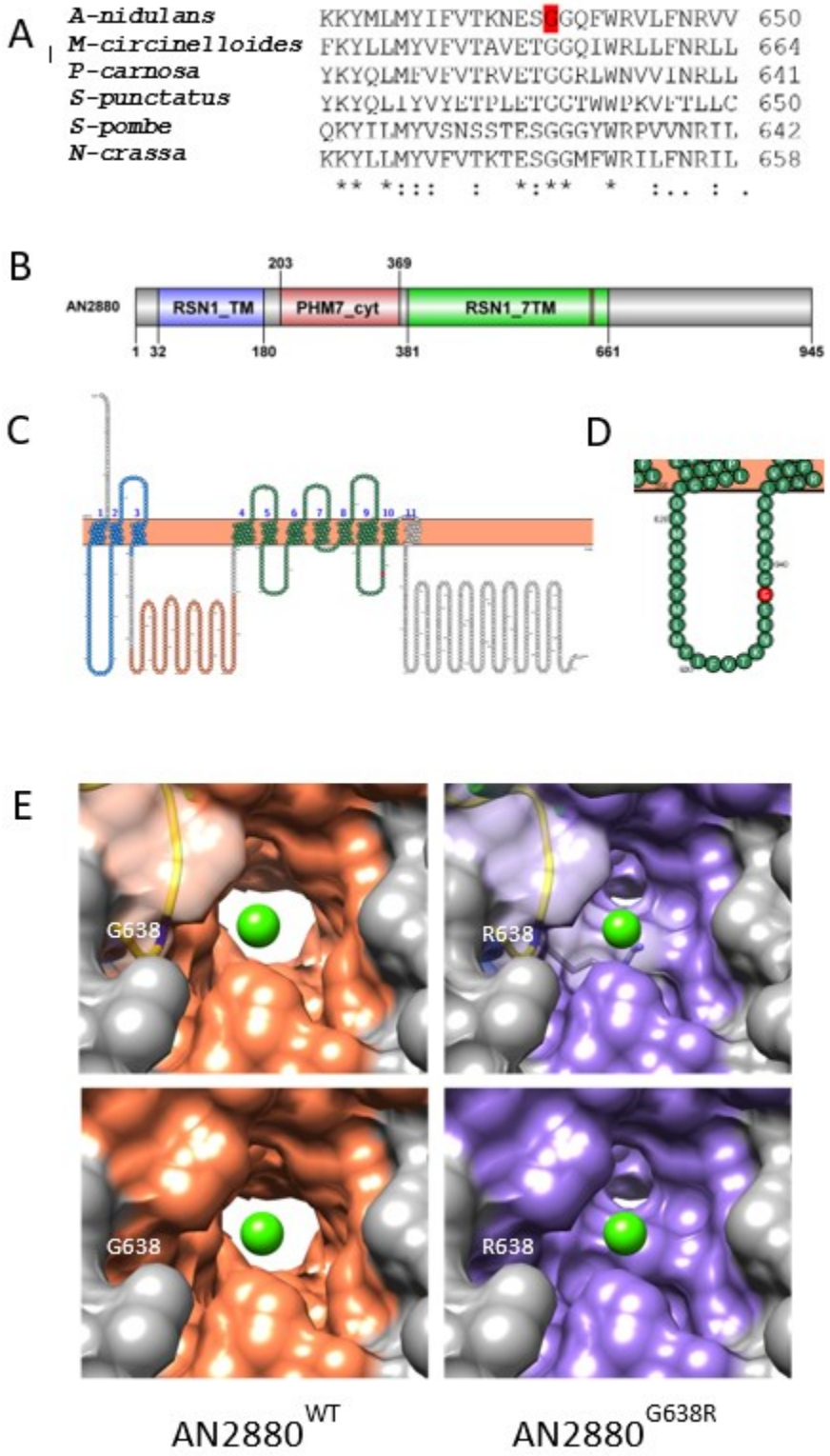
A
A-nidulans KKYMLMYIFVTKNESGGQFWRVLFNRVV 650
M-circinelloides FKYLLMYVFVTAVETGGQIWRLLFNRLL 664
P-carnosa YKYQLMFVFVTRVETGGRLWNVVINRLL 641
S-punctatus YKYQLIYVYETPLETGGTWWPKVFTLLC 650
S-pombe QKYIIMYVSNSSTESGGGYWRPVVNRIL 642
N-crassa KKYLLMYVFVTKTESGGMFWRILFNRIL 658
B
AN2880
RSN1_TM
PHM7_cyt
RSN1_7TM
203
369
1
32
180
381
661
945
C
D
E
G638
R638
G638
R638
AN2880WT
AN2880G638R

Figure 3

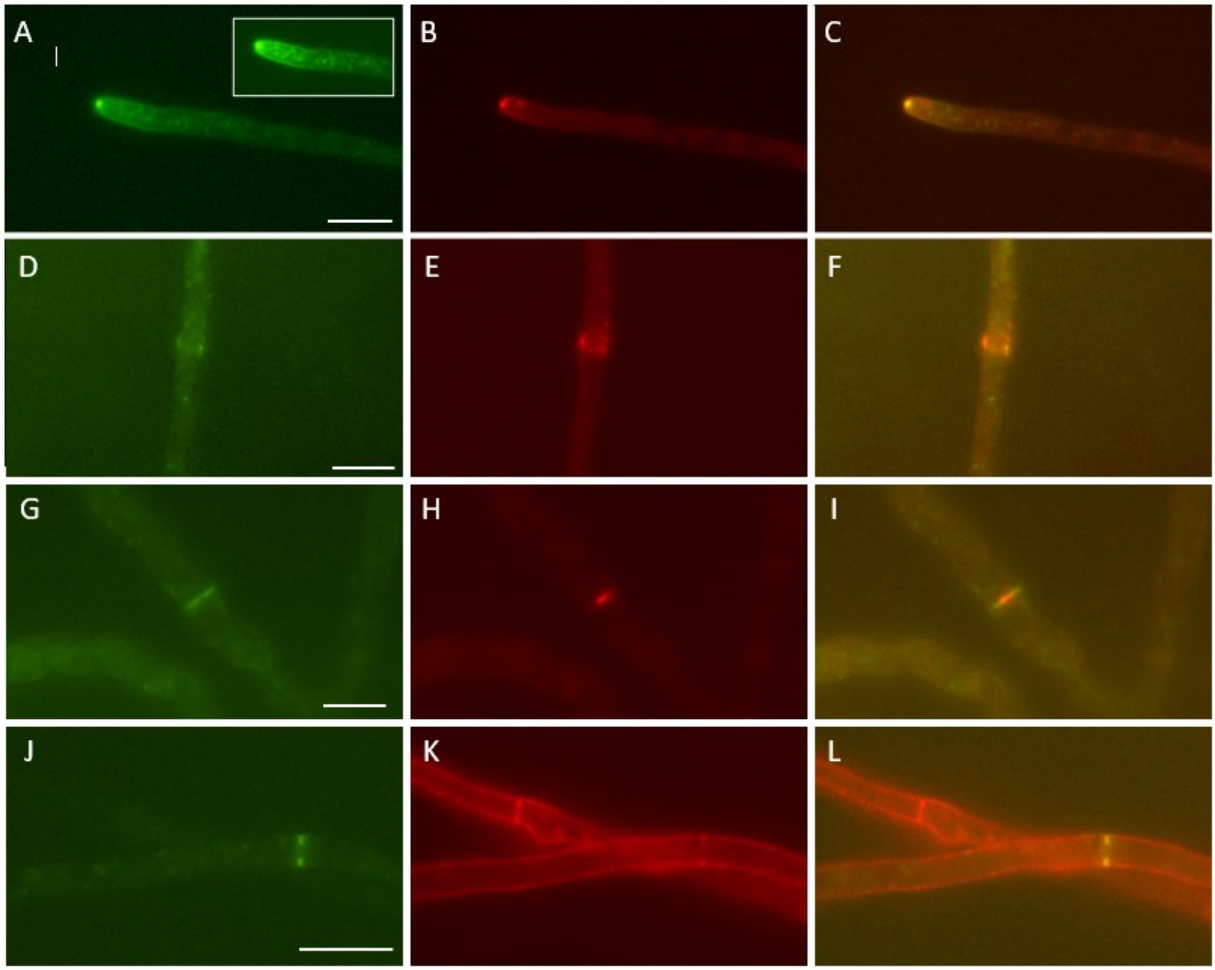

Figure 4

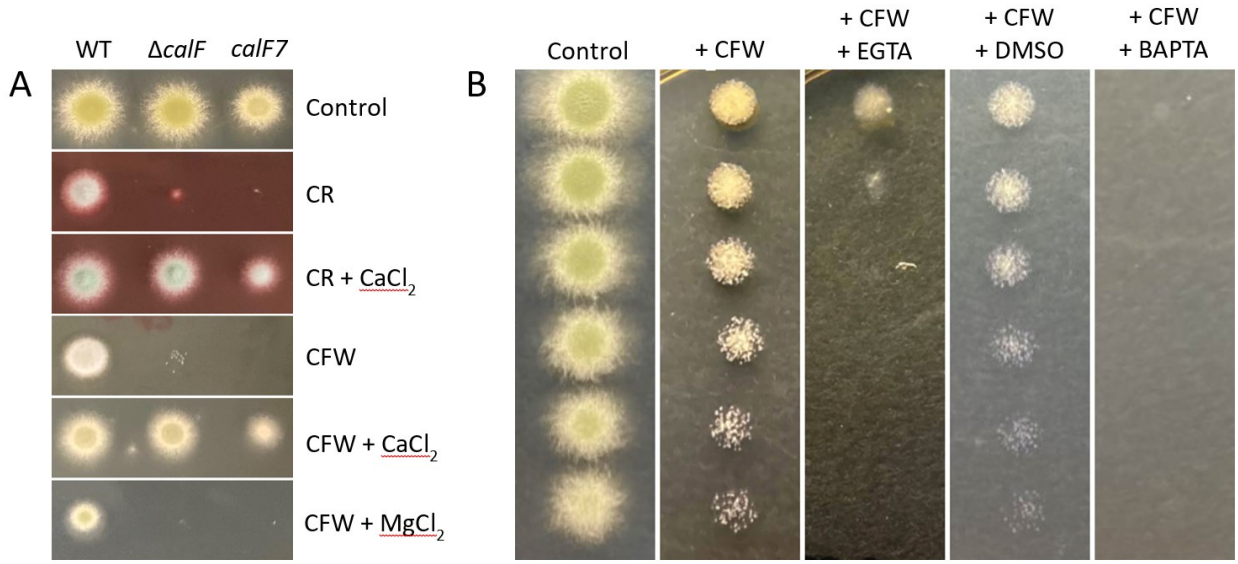
A
WT
ΔcalF
calF7
Control
CR
CR + CaCl2
CFW
CFW + CaCl2
CFW + MgCl2
B
Control
+ CFW
+ CFW
+ EGTA
+ CFW
+ DMSO
+ CFW
+ BAPTA